O. Putzeys, A. Bar-Ilan, G. Rein, A.C. Fernandez-Pello, D.L. Urban. "The role of secondary char oxidation in the transition from smoldering to flaming", Proceedings of the Combustion Institute 31 (2), pp. 2669-2676, 2007.
http://www.era.lib.ed.ac.uk/handle/1842/1152

The role of secondary char oxidation in the transition from smoldering to flaming

Olivier Putzeys, Amnon Bar-Ilan, Guillermo Rein, A. Carlos Fernandez-Pello
University of California Berkeley, CA USA

David L. Urban
NASA Glenn Research Center, OH USA

Corresponding Author contact information**:**
Prof. A. Carlos Fernandez-Pello
Mechanical Engineering
6105A Etcheverry Hall
University of California
Berkeley, CA 94720-1740 USA
Phone: (510) 642-6554
Fax: (510) 642-6163
Email: ferpello@me.berkeley.edu

Abstract

The transition from forward smoldering to flaming in polyurethane foam is observed using in-depth thermocouples and ultrasound probing. The experiments are conducted with small parallelepiped samples vertically placed in an upward wind tunnel. Three of the vertical sample sides are maintained at elevated temperature and the fourth is exposed to an upward oxidizer flow and a radiant heat flux. An ultrasound probing technique is used to measure the line-of-sight average permeability of the sample at the same heights as the thermocouples. The smolder front propagation is tracked by both the thermocouples and ultrasound data, which show an increase in temperature and permeability upon passage of the smolder front. The permeability data also show that the transition to flaming is preceded by rapid fluctuations in permeability in the char region below the smolder front, indicating the formation of pores by secondary char oxidation. The pores provide locations for the onset of gas-phase ignition (i.e. transition to flaming). The results from all the tests indicate that the formation of pores is a necessary but not sufficient condition for the transition to flaming. Two novel measures of the intensity of the secondary char oxidation are introduced: the time derivative of permeability, and the secondary char oxidation velocity. The time derivative of permeability, which provides a measure of the pore formation rate, is found to increase as the oxygen concentration and/or radiant heat flux increase, and to indicate the likelihood of the transition to flaming. The permeability data offers a means to track the propagation of the secondary char oxidation, and to calculate the secondary char oxidation velocity, which is found to be strongly correlated to the transition to flaming. A simplified energy balance model is able to predict the dependence of the secondary char oxidation velocity on oxygen concentration and radiant heat flux.

Keywords: smoldering; transition to flaming; secondary char oxidation; polyurethane foam; ultrasound.

1. Introduction

The transition from smoldering to flaming is of interest for both fundamental research and fire safety applications. It is a complex problem that involves heat and mass transport and fluid flow in porous media, and heterogeneous smolder reactions that provide gaseous fuel and heat to trigger gas-phase reactions (flaming). The danger of smoldering is clearly observable by the fact that 25% of residential fire deaths in the United States are caused by smolder-originated fires [1].

The transition to flaming is much more likely to occur in the forward smoldering configuration, in which the oxidizer flows in the same direction as the smolder propagation [2,3], and the hot char left behind by the smolder reaction receives a fresh supply of oxidizer and can undergo a highly exothermic secondary char oxidation (SCO), potentially leading to a transition to flaming. Most of the work on transition to flaming has used cellulosic materials or polyurethane foam, with variable fuel sample sizes, orientations, and oxygen concentrations [4-9]. These studies have shown that the fuel samples must be fairly large (i.e. self-insulating) in order to produce a transition to flaming in air. Otherwise, the smolder reaction and transition to flaming must be assisted by using elevated oxygen concentrations or external heating [9].

Smoldering generally occurs in the interior of opaque porous materials, and is therefore difficult to observe non-intrusively. Ultrasound probing offers a non-intrusive means of monitoring the changing structure of a smoldering sample's interior and tracking the smolder front, because the smolder reaction leaves behind a char of higher permeability than the unreacted foam [10,11]. Tse et al. developed an ultrasound imaging technique [11] to determine the permeability of a sample from the attenuation of the ultrasound signal. The char was found to continue reacting (SCO) after the passage of the smolder front, resulting in the formation of pores in the char region, thereby allowing greater oxidizer supply and potentially triggering a gas-phase ignition. The study of Tse et al. is the only extensive work to date using ultrasound to study the transition to flaming, however it was not able to capture in high temporal resolution the events leading to the transition, due to data acquisition limitations. The current study seeks to remove these limitations in order to gain further insight into the transition from smoldering to flaming.

More specifically, the high-speed ultrasound system presently used permits the introduction of two novel measures of the intensity of the SCO: the time derivative of permeability, and the propagation velocity of the SCO wave.

2. Experiment

2.1. Experiment background

The current study is part of a NASA-sponsored program to study the transition from smoldering to flaming in environmental conditions encountered in spacecraft facilities, i.e. microgravity, low velocity gas flows of varied oxygen concentrations. The microgravity experiments were initially planned for the International Space Station, and therefore the sample size had to be limited for safety and launch mass reasons, to dimensions of 50 x 50 x 125 mm. Smoldering is a weak reaction that propagates through a balance between the heat generated, the heat transferred ahead of the smolder front and heat lost to the surroundings. Preliminary experiments showed that the heat losses were too great with this sample size for the smolder reaction to propagate without assistance. Therefore, the smolder reaction had to be assisted with elevated oxygen concentrations, and limiting the heat losses with an external radiant heat flux on the free sample surface, and guard heaters on the sample holder walls [9].

2.2. Experimental apparatus

The experimental apparatus, shown schematically in Fig. 1, is the same as that used by Bar-Ilan et al. [9] (with the addition of the ultrasound probing system), who describe the equipment in more detail. The vertically oriented parallelepiped foam sample is heated on three of its surfaces, and the free fourth surface is exposed to an upward forced oxidizer flow parallel to the surface. Smolder is initiated at the bottom of the sample and the smolder reaction propagates upward in the same direction as the oxidizer flow (buoyant and forced), i.e., forward smoldering.

In all testing, the fuel samples were open-celled, non-fire retarded, flexible polyurethane foam of density 26.5 kg/m^3, porosity 0.975, and dimensions 50 x 50 x 125 mm. The outer surfaces of the back and side walls of the sample holder have guard heaters set to 200 ºC [9]. An infrared radiant heater is mounted opposite the sample to counter convective heat losses from the exposed sample surface to the forced duct flow (0.5 m/s for all tests).

To initiate the smolder reaction, the bottom face of the sample is in contact with an electrically heated ceramic honeycomb igniter of area 50 x 50 mm, set to a power of 23.25 W, which was determined to be the optimal power for smolder ignition based on previous testing. During the tests, there is a forced flow of oxidizer through the igniter, and into the porous fuel sample at a flow rate of 13.4 cc/s, which was determined to be the optimal internal flow rate for smolder ignition and propagation from previous testing.

Six type-K thermocouples are located along the centerline of the sample at distances from the igniter/fuel interface of: 0, 20, 40, 60, 80 and 100 mm. The thermocouples are 0.84 mm diameter sheathed-grounded probes, inserted through the back of the sample. An Environmental Scanning Electron Microscope (ESEM), Philips model XL-30, is used to obtain images of the virgin foam and char microstructures.

2.2.1. Ultrasound Probing System

The ultrasound technique follows the same approach as that of Tse et al. [11] and uses speaker-microphone pairs to track the progress of the smolder reaction (because the char is more permeable than the virgin foam) and to observe the evolution of the char. The acoustic attenuation coefficient α of the porous medium can be approximated [11] as being inversely proportional to the square root of the permeability K, by $\alpha = A/K^{1/2}$, where A is a constant dependant on the ultrasonic frequency, the medium porosity, and several fluid properties, giving:

$$\frac{V}{V_0} = e^{-\frac{AL}{\sqrt{K}}} \tag{1}$$

where V is the received signal amplitude, V_0 is the unattenuated signal amplitude, calibrated for signal losses due to beam expansion and the waveguides (described below), and L is the sample thickness. This technique provides a measure of the line-of-sight average permeability, due to the fact that the structure of the sample at a given height is not uniform (i.e. there is always a thin layer of unburned foam on the edges). The system was calibrated with the foam used in the present study and a lower density (16.5 kg/m^3) polyurethane foam, whose permeabilities were found to be 5.23 x 10^{-9} m^2 and 8.70 x 10^{-9} m^2, respectively, using Darcy's law for fluid flow through a porous medium: $u = -K/\mu \, \Delta P/\Delta x$, where u is the bulk fluid velocity, μ is the viscosity, and ΔP is the pressure drop, and Δx is the length.

As shown in Fig. 1, the speaker-microphone pairs are positioned at the same heights on the sample centerline as the top five thermocouples. The ultrasound signals pass through holes of 10 mm diameter on the sides of the sample holder. The speakers and microphones (Murata® models MA40S4S and MA40S4R, respectively) are of 10 mm diameter. In order to protect the speakers and microphones from excessive heat, they are separated from the foam sample sides by copper tube waveguides (50 mm long and 10 mm inner diameter), which serve as conduits for the ultrasonic signal. A more detailed description of the ultrasound system equipment is in [11]. The major modification of this system for the present work has been to increase the data acquisition rate to 2 Hz at each probing location.

2.3. Experiment Procedure

Tests are conducted at various radiant heat fluxes and oxygen concentrations of the duct and internal flows. The igniter is activated when the guard heaters reach their set point temperature. The smolder reaction is first initiated using air in both the duct and internal flows. The igniter is turned off when the smolder front has propagated away from the igniter, as indicated by the thermocouple at 40 mm passing 300 ºC. In order to ensure that the transition to flaming is not directly influenced by the igniter, the igniter is allowed to cool to 250 °C, at which point the internal and external flows are simultaneously

enriched to the nominal oxygen mole fraction. If the smolder reaction reaches the end of the sample without a transition to flaming, the test is stopped.

3. Results and Discussion

3.1. Transition to flaming: thermocouple and ultrasound probing results

A set of experiments was performed varying the oxygen mole fraction, between 0.25 and 0.40, and the radiant heat flux, at 8.00 or 8.75 kW/m^2. Tests performed at 0.35 and 0.40 oxygen mole fraction all underwent transition to flaming, while none of the tests at 0.25 and 0.30 oxygen mole fraction transitioned to flaming, consistent with [9].

Characteristic plots of temperature and line-of-sight average permeability versus time for a test that transitioned from smoldering to flaming are shown in Fig. 2a and b, respectively, for a test at 0.35 oxygen mole fraction, and 8.00 kW/m^2. Temperature and permeability data from tests at other conditions were qualitatively similar. The initiation and propagation of the smolder reaction is seen in the temperature traces of the thermocouples at 20 and 40 mm. The igniter is shut off at 715 s, and the smolder reaction continues to propagate vertically up the sample, as seen in the temperatures profiles of the upper four thermocouples, which exhibit typical forward smolder behavior [3,12].

The propagation of the smolder front is also seen in the permeability data in Fig. 2(b), as each of the permeability traces exhibits a general increase as the smolder wave passes. Interestingly, for each ultrasound probing location, the permeability first slightly decreases just prior to increasing sharply. The first dip in permeability begins when the temperature is in the range of 240-260 ºC, and it occurs about 20-25 seconds, and 15-20 ºC, before the trend reverses and the permeability begins to rise. It is possible that the decrease in permeability is due to condensed pyrolysis products clogging the pores, however clogged pores have not been observed in post-test sample inspection. Instead, the decrease in permeability is likely caused by the "break-line" interface [13], as seen in Fig. 3, which shows a cross section of a sample

purged with nitrogen to extinguish the smolder reaction. This interface is formed between the thermally degraded foam (more brittle but structurally similar to the virgin foam, whose microstructure is shown in Fig. 4a) and the char region (microstructure shown in Fig. 4b). As the convex interface enters the probing path, ultrasound reflection at the boundary [14] probably attenuates the ultrasound wave, producing the apparent decrease in permeability.

The first increase in permeability begins when the temperature is in the range of 250-280 ºC, which corresponds to the onset of pyrolysis for polyurethane foam [15]. The pyrolysis front, which precedes the oxidation front in the forward smoldering configuration [2,3], vaporizes a portion of the fuel, causing a local increase in permeability. The oxidation front that follows consumes additional solid fuel, further increasing the permeability, and leaves behind a low-density char (Fig. 4b). After the local temperature has passed 300 ºC, i.e. after the leading edge of the smolder wave [3,12] has passed that location, there are fluctuations in the measured permeability in the char region. Post-test inspection of samples, and the cross-section of the smolder-extinguished sample in Fig. 3, show that in the char region there are pores with walls partially consisting of melted skins of char, shown in the ESEM image in Fig. 4(c). A melted char skin is also apparent at the bottom of the sample (Fig. 3), likely due to heating from the igniter. Although char as it is traditionally defined cannot melt, the char produced from smoldering likely contains some partially reacted polymer that allows it to exhibit a melting behavior. It appears that the char strands are melted together into skins, which have also been observed in [16], where they are described as “solidified films” and suggested as the cause of the observed decreases in permeability. These skins can lower the measured permeability by attenuating the ultrasound signal by reflection [14]. However, the char is being consumed simultaneously, which tends to increase the local permeability. These competing effects most likely cause the fluctuations in measured permeability, as one effect dominates over the other and then vice-versa, depending on the local temperature and availability of oxygen. High temperature alone would tend to melt and pyrolyze the char, however if sufficient oxygen is present near the char surface, char consumption by oxidation would be promoted.

After the flows are enriched to the nominal elevated oxygen mole fraction (0.35 for this test) at 962 s, the temperature at 100 mm begins to increase more quickly (Fig. 5a), indicating an intensifying smolder reaction at that location. Simultaneously, the permeability at 100 mm increases substantially (Fig. 5b), as a result of rapid fuel mass loss. Subsequently, the temperatures at 80, 60, and 40 mm increase, showing the downward propagation of a SCO wave, corroborated by the permeability profiles beginning to fluctuate at 100, 80, 60, and 40 mm, chronologically. During this period, the permeability data shows higher-frequency fluctuations than were observed before oxygen enrichment. Visual observation of tests (the pores sometimes emerge onto the free surface of the sample) and post-test inspection of smolder-extinguished samples such as Fig. 3 indicate that the intense SCO rapidly creates large pores with walls of melted char skins.

The permeability at 40 mm begins to change sharply at 992 s, first decreasing and then increasing, indicating the formation of a pore due to stronger SCO. Close inspection of the temperature data in Fig. 5(a) reveals that the temperature at 40 mm is the first to jump sharply, at 995.4 s, indicating a transition to flaming near that location. At this time, the smolder front is around 100 mm; therefore, the transition to flaming occurred in the char region behind the smolder front, in agreement with observations of previous studies [7-9]. The corroboration of the temperature and permeability data strongly suggests that the transition to flaming occurred in the pore that was forming at 40 mm. At 995.9 s, the temperature at 20 mm jumps sharply, showing that the flame has propagated downwards in the interior of the sample. After the transition to flaming, the permeabilities at all probing locations fluctuate drastically due to the rapid mass consumption and simultaneous foam melting. The flame quickly attaches itself to the unburned foam at the edges of the exposed sample surface. The erratic temperature profiles after 1000 s are due to the manual extinguishment using a jet of carbon dioxide.

The temperature and permeability histories for tests that did not transition to flaming (i.e. at 0.25 and 0.30 oxygen mole fraction) are very similar to Fig. 2a and b except for the variations near the transition to flaming. The tests also show rapid fluctuations in permeability and increasing temperatures due to the SCO. However, the peak temperatures in these tests are lower than those for 0.35 oxygen mole fraction in

Fig. 5a, and they begin to decrease when most of the usable fuel has been consumed, as confirmed by post-test sample inspection. Apparently, at the lower oxygen concentrations the SCO does not generate sufficient heat to trigger a gas-phase ignition.

Post-test sample inspection and the permeability data show that large pores are formed in all test samples, for different oxygen concentrations and radiant heat fluxes. Therefore, the formation of large pores is a necessary but not sufficient condition for the transition to flaming. Large pores are required for gas-phase ignition because surface quenching by heat loss and removal of radical species is promoted in small pores [2]. Figures 4a and c show that virgin foam and char have pores on the order of 500 μm, while the SCO creates much larger pores, on the order of 1-2 cm (Fig. 3), which enable gas phase reactions to undergo thermal runaway, leading to ignition.

While the formation of large pores does not necessarily lead to ignition, the time derivative of permeability can provide a more reliable indication of the likelihood of a transition to flaming. The time derivative of permeability is a novel measure of the pore formation rate and the SCO intensity, obtainable with the current high-speed ultrasound probing system. Fig. 6 shows the maximum time derivative of permeability (before the transition to flaming) for tests at varying oxygen concentration and radiant heat flux. The data shows that pores form more rapidly at increased oxygen concentration and/or increased radiant heat flux, and that the time derivative of permeability appears to be correlated to the transition to flaming. From Fig. 6 it appears that there is a time derivative of permeability corresponding to the threshold oxygen concentration for the transition to flaming; for this experimental configuration the value is approximately 2×10^{-9} m^2/s.

3.2. Velocity of Secondary Char Oxidation Wave

As described above, the arrival of the SCO wave at an ultrasound probing location is indicated by a sharp change in permeability. Therefore, the permeability data offer a novel means of calculating the downward propagation velocity of the SCO, which cannot be done using the temperature data because its

arrival is difficult to identify precisely from the temperature traces. The resulting SCO velocities are shown in Fig. 7 for tests at varying oxygen mole fraction and radiant heat flux. The uncertainties in the calculated velocity data are due to uncertainties in both the distance measurement (the spatial resolution of the ultrasonic transducers is 10 mm) and the time measurement (the ultrasound data acquisition rate is 2 Hz). The uncertainty is greater at higher velocities because the uncertainty in time is relatively larger for shorter time intervals. It can be seen that increasing the oxygen concentration increases the propagation velocity significantly, and the dependence is not linear. Increasing the radiant heat flux from 8.00 to 8.75 kW/m^2 has in general a slightly positive effect on the SCO velocity.

This paper introduces a method of modeling the propagation velocity of the SCO, using a simplified steady-state energy balance on a control volume containing the reaction zone. The analysis is based on previous theoretical works on one-dimensional opposed smoldering [10,16,17]. The SCO propagation is similar to opposed smoldering in that it moves counter to the direction of oxidizer flow. The analysis assumes that the propagation velocity depends on a balance of the heat generation and external heat input versus the heat losses and the energy required to heat the incoming solid char and oxidizer flow to the temperature of SCO. To calculate the heat generation, it is assumed that all the oxygen is consumed at the reaction front. The energy balance model of [10,16,17] has been extended to include the non-negligible component of the oxidizer flux due to the relatively high velocity of the SCO. The analysis includes the radiant heat flux and estimates of the heat losses due to convection on the free sample surface and conduction on the three unexposed sample sides, yielding the following expression for the SCO velocity:

$$u_{sco} = \frac{Y_{O_2}\rho_g u_i Q_{sco} - \rho_g u_i c_g \left(T_{sco} - T_c\right) + \left(\dot{Q}''_{rad} - \dot{Q}''_{loss}\right) A_L / A_C}{-Y_{O_2}\rho_g Q_{sco} + \left(\rho_g c_g + \rho_s c_s \left(1-\phi_c\right)\right)\left(T_{sco} - T_c\right)} \tag{2}$$

where Y_{O2} is the mass fraction of oxygen, ρ_g (1.2 kg/m^3) and ρ_s (1034 kg/m^3) are the densities of the gas and solid char, u_i (5.4 mm/s) is the internal flow velocity, Q_{sco} is the heat of SCO per mass of oxygen consumed, c_g (1.1 kJ/kg-K) and c_s (1.7 kJ/kg-K) are the specific heats of the gas and solid char, T_{sco} (400

ºC) is the temperature of SCO, T_c (300 ºC) is the char temperature, $\dot{Q}''_{rad}$ is the radiant heat flux, $\dot{Q}''_{loss}$ is the total heat loss flux due to convection and conduction [9], ϕ_c (0.989) is the porosity of the char, and A_L/A_C (0.5) is the ratio of the lateral to the cross-sectional area of the SCO zone. The heat of SCO is not well defined, and was therefore optimized in this analysis to give the best fit with the experimental data; the resulting value is 3050 kJ/kg-O_2. The last term in the denominator of Eq. (2) could help account for the high temperatures generated by SCO, because the energy required to heat the incoming char is much less than that required to heat the unburned foam entering the primary smolder front, due to the higher porosity and smaller temperature difference.

The results of Eq. (2) are plotted versus the experimental values in Fig. 7. The simplified analysis predicts fairly well the effects of oxygen mole fraction and radiant heat flux on the SCO velocity, indicating that the velocity depends essentially on the balance between heat generation and heat losses, and that the reaction is oxygen-limited. Increasing the oxygen concentration, which allows more heat generation by char oxidation, increases the propagation velocity. Opposed smoldering velocities increase linearly with oxygen concentration [10,16,17]. However, both the experimental data and the analysis show that the dependence of the SCO velocity on the oxygen concentration is not linear; that is, the velocity increases more quickly as the oxygen concentration increases. Mathematically, this is due to the presence of the first term in the denominator of Eq. (2). This term represents the component of oxygen flux to the reaction zone due to the downward velocity of the SCO, which is approximately one to two orders of magnitude greater than typical opposed smoldering velocities [10,16].

The transition to flaming has been shown to occur in the char region behind the smolder front, and not to be the result of an accelerating smolder front velocity [7-9]. Instead, the present results indicate that the transition to flaming is strongly correlated to the propagation velocity of the SCO. From Fig. 7, it appears that the SCO velocity corresponding to the critical oxygen concentration for the transition to flaming, for this experimental configuration, is in the range 2.5 – 3 mm/s. At SCO velocities greater than 3 mm/s, the high rate of heat generation raises the local temperature sufficiently to trigger the transition to flaming.

4. Conclusions

The ultrasound probing system is able to track the propagation of both the smolder front and the SCO. The permeability data shows that the transition to flaming is preceded by large fluctuations in sample permeability, indicating the formation of pores and melted char skins due to SCO. The temperature and permeability data indicate that the transition to flaming occurs in pores formed by SCO in the char region behind the smolder front. The role of the SCO in the transition to flaming has been shown to be three-fold: it provides the fuel, heat, and favorable sites (large pores) for gas-phase ignition.

The time derivative of permeability provides a novel measure of the pore formation rate and the intensity of the SCO. The data shows that increased oxygen concentration or radiant heat flux increases the pore formation rate, and favors the transition to flaming. The time derivative of permeability corresponding to the threshold oxygen concentration for the transition to flaming has been found to be approximately 2×10^{-9} m^2/s. While pore formation is a necessary but not sufficient condition for the transition to flaming, the results indicate that the pore formation rate, represented qualitatively by the time derivative of permeability, is strongly correlated with the transition to flaming.

The permeability data offers a novel means to track the propagation of the secondary char oxidation, and to calculate the SCO velocity. The SCO velocity corresponding to the critical oxygen concentration for the transition to flaming has been found to be in the range 2.5 – 3 mm/s. The presented energy balance model is able to predict the effects of oxygen concentration and radiant heat flux on the SCO velocity. The results indicate that the transition to flaming is strongly correlated with the SCO velocity, rather than an accelerating smolder front.

Acknowledgements

The authors would like to thank Robin Titus, Manuel Reyes and Danny Leang for their help conducting the experiments, and the STAF engineering team at NASA Glenn Research Center for their engineering support.

References

[1] J.R. Hall, *The Smoking-Material Fire Problem*, National Fire Protection Association, 2004.
[2] T.J. Ohlemiller, *Prog. Energy Combust. Sci.* 11 (4) (1985) 277-310.
[3] J.L. Torero, A.C. Fernandez-Pello, *Combust. Flame* 106 (1-2) (1996) 89-109.
[4] K.N. Palmer, *Combust. Flame* 1 (2) (1957) 129-153.
[5] M.G. Ortiz-Molina, T.Y. Toong, N.A. Moussa, G.C. Tesoro, *Proc. Combust. Inst.* 17 (1979) 1191-1200.
[6] T.J. Ohlemiller, *Combust. Flame* 81 (3-4) (1990) 354-365.
[7] S.D. Tse, A.C. Fernandez-Pello, K. Miyasaka, *Proc. Combust. Inst.* 26 (1996) 1505-1513.
[8] C.Y.H. Chao, J.H. Wang, *Combust. Flame* 127 (4) (2001) 2252-2264.
[9] A. Bar-Ilan, O.M. Putzeys, G. Rein, A.C. Fernandez-Pello, D.L. Urban, *Proc. Combust. Inst.* 30 (2005) 2295-2302.
[10] J.L. Torero, A.C. Fernandez-Pello, M. Kitano, *Combust. Sci. Technol.* 91 (1-3) (1993) 95-117.
[11] S.D. Tse, R.A. Anthenien, A.C. Fernandez-Pello, *Combust. Flame* 116 (1-2) (1999) 120-135.
[12] A. Bar-Ilan, G. Rein, A.C. Fernandez-Pello, J.L. Torero, D.L. Urban, *Exp. Therm. Fluid Sci.* 28 (7) (2004) 743-751.
[13] F.E. Rogers, T.J. Ohlemiller, 11 (1) (1980) 32-44.
[14] J.F. Allard, *Propagation of Sound in Porous Media*. Elsevier Science Publishers, England, 1993.
[15] C.Y.H. Chao, J.H. Wang, *J. Fire Sci.* 19 (2) (2001) 137-156.
[16] A. Bar-Ilan, G. Rein, D. C.walther, A.C. Fernandez-Pello, J.L. Torero, D.L. Urban, *Combust. Sci. Technol.* 176 (12) (2004) 2027-2055.
[17] S.S. Dosanjh, P.J. Pagni, A.C. Fernandez-Pello, *Combust. Flame* 68 (2) (1987) 131-142.

List of Figure Captions

Fig. 1. Schematic of the experimental apparatus.

Fig. 2. Characteristic histories of (a) temperature and (b) line-of-sight average permeability, for a test that transitioned to flaming. The legend indicates the height above the igniter/fuel interface.

Fig. 3. Cross-section of sample tested at 0.35 oxygen mole fraction, and 8.00 kW/m^2 radiant heat flux. The smolder was extinguished with a nitrogen purge 30 seconds after oxygen enrichment.

Fig. 4. ESEM images of (a) virgin polyurethane foam (b) char prior to secondary char oxidation (c) melted char skin.

Fig. 5. Detailed histories of (a) temperature and (b) line-of-sight average permeability, of the secondary char oxidation and transition to flaming, for the test shown in Fig. 2.

Fig. 6. Maximum time derivative of permeability (10^{-9} m^2/s), before the transition to flaming, for varying oxygen mole fraction and radiant heat flux.

Fig. 7 Experimental and predicted downward propagation velocity of the secondary char oxidation for varying oxygen mole fraction and radiant heat flux.

Figures

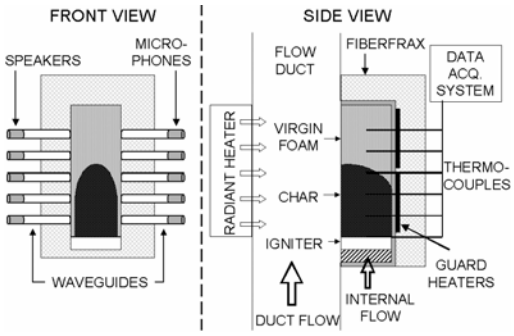

Fig. 1

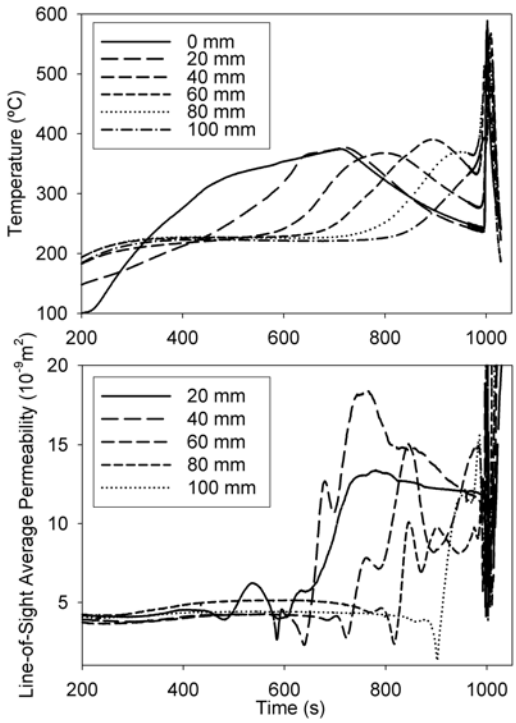

Fig. 2 a and b

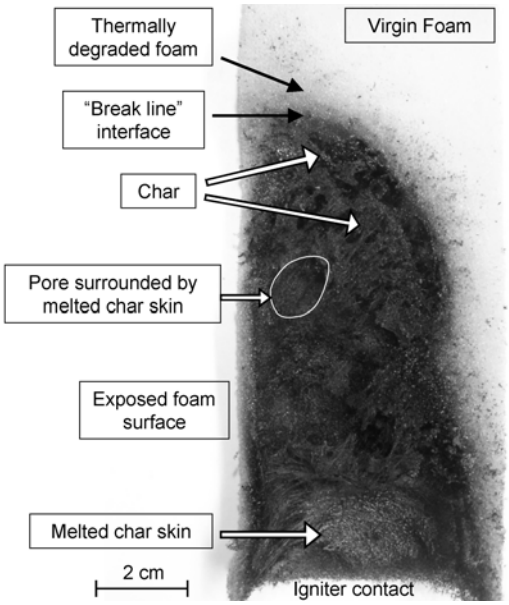

Fig. 3

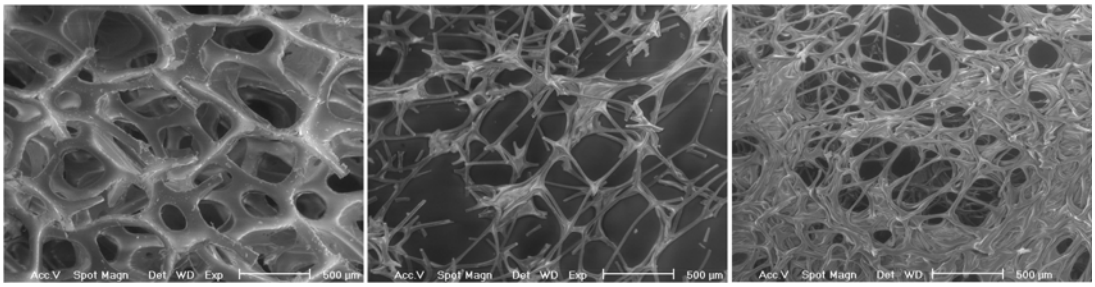

Fig. 4 a, b and c

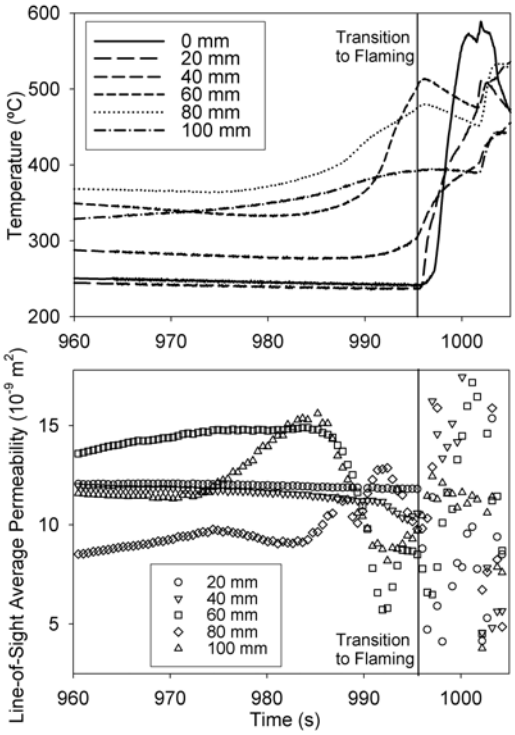

Fig. 5 a and b

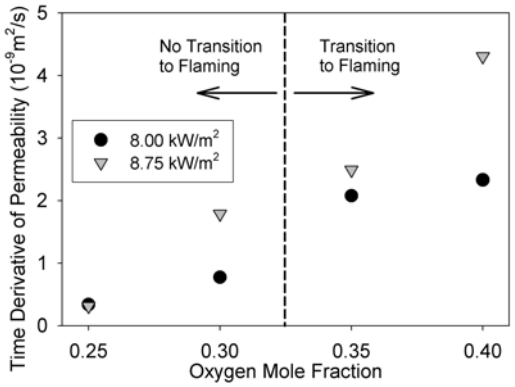

Fig. 6

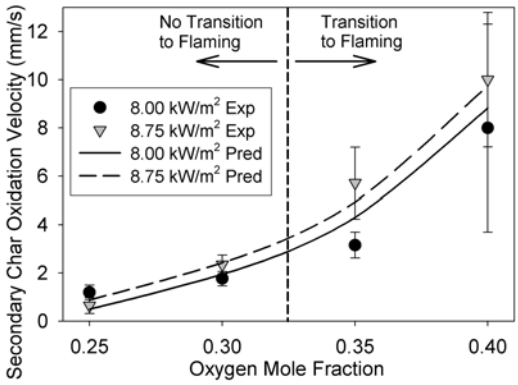

Fig. 7